Mass-Resolved Resonance Enhanced Ionization Study of Complicated Excited Electronic States of Rb₂ near 430 nm and Their Predissociation Dynamics

Yonghoon Lee,[†] Sungyul Lee,[‡] and Bongsoo Kim*,[§]

Advanced Photonics Research Institute, Gwangju Institute of Science and Technology, Gwangju 500-712, Korea, College of Environmental Science and Applied Chemistry (BK21), Kyunghee University, Kyungki-do 449-701, Korea, and Department of Chemistry, KAIST, Daejeon 305-701, Korea

We have investigated the Rb₂ 430 nm system by resonance enhanced two-photon ionization and photofragment yield spectroscopy. Four electronically excited states have been assigned, and their two-channel (fast and slow) predissociation has been observed. For the $3\,^1\Pi_u$, $3\,^1\Sigma_u^+$, $3\,^3\Pi_u(0_u^+)$, and $3\,^3\Pi_u(1_u)$ states, electronic term values (T_e) and vibrational constants (ω_e and $\omega_e x_e$) have been determined. For the predissociation dynamics, we have observed the fast predissociation threshold between the isotopically shifted $3\,^1\Pi_u$ v′ = 14 levels of ^{85}Rb₂ and ^{85}Rb^{87}Rb where the $4\,^2D_{5/2} + 5\,^2S_{1/2}$ atomic fine-structure limit is located. The $1\,^3\Delta_u$ state corresponding to the $4\,^2D_{5/2} + 5\,^2S_{1/2}$ atomic fine-structure limit has been assigned to the predissociating perturber responsible for the fast channel. Also, we have found that the fast channel branches out into two finer product channels due to long-range potential crossing.

1. Introduction

Rb₂, one of the heavy alkali metal diatomic molecules, has very dense excited electronic states in the region between 20000 cm⁻¹ and its ionization potential.[1] This situation enhances perturbations among the excited states with the consequence that the spin-forbidden triplet−singlet electronic transitions are observed with strong intensity,[2] the predissociation occurs through multiple channels,[3−5] and the angular momentum coupling scheme approaches Hund's case (c).[6]

For the ground X $^1\Sigma_g^+$ electronic state of Rb₂, the potential energy curve up to v″ = 113 was experimentally determined very accurately.[7] For the excited states, the $2\,^1\Sigma_g^+$, $1\,^1\Pi_g$, $1\,^1\Sigma_u^+$, and $1\,^1\Pi_u$ states corresponding to the 5s + 5p atomic limit were studied using high-resolution Fourier transform (FT) spectroscopy, and their potential curves were determined.[8−10] For the higher-lying excited states, Tsi-Zé and San-Tsiang observed band spectra near 475 and 430 nm and reported T_e and ω_e values of the $2\,^1\Pi_u$ and $3\,^1\Pi_u$ states in 1937.[11] Since their work, several studies on the predissociation of the $2\,^1\Pi_u$ and $3\,^1\Pi_u$ states have been reported.[3−5,12,13] Recently, the $2\,^3\Pi_u$ ← X $^1\Sigma_g^+$ triplet−singlet transition near 500 nm and the $1\,^1\Delta_g$ ← X $^1\Sigma_g^+$ electric quadrupole transition near 540 nm have been reported.[2,14]

The Rb₂ 430 nm system is the highest spectral region experimentally investigated so far. In this region, the vibronic structure[11] and the predissociation[3−5] of the $3\,^1\Pi_u$ state were reported. On the predissociation dynamics, Breford and Engelke reported that the $3\,^1\Pi_u$ state was predissociated into two different channels measuring the laser induced fluorescence of Rb₂ $3\,^1\Pi_u$ → X $^1\Sigma_g^+$ and the Rb atomic fluorescence centered at D1 ($5\,^2P_{1/2}$ → $5\,^2S_{1/2}$, 794.8 nm) and D2 ($5\,^2P_{3/2}$ → $5\,^2S_{1/2}$,

780.0 nm) lines.[3] They observed both D1 and D2 line emissions. In particular, the D1 line emission appeared strongly above the sharp energy threshold of about 429.5 nm. They interpreted that these D1 and D2 emissions are due to the production of excited Rb atoms by the predissociation of the Rb₂ $3\,^1\Pi_u$ state via two different channels; one produces Rb $5\,^2P_{3/2}$ and Rb $5\,^2S_{1/2}$ fragments through the repulsive $2\,^3\Sigma_u^+$ state, and the other becomes available when the excitation wavelength is shorter than 429.5 nm producing Rb $4\,^2D_{3/2}$ and Rb $5\,^2S_{1/2}$ fragments. The excited Rb $4\,^2D_{3/2}$ fragment can generate D1 line emission by the cascade of $4\,^2D_{3/2}$ → $5\,^2P_{1/2}$ → $5\,^2S_{1/2}$ transitions. Breford and Engelke proposed that the predissociating perturber of the second channel was the $2\,^3\Pi_u$ continuum state corresponding to the $4\,^2D_{3/2} + 5\,^2S_{1/2}$ limit.[3] Recently, Zhang et al.[4] and Gador et al.[5] proposed that the continuum $1\,^3\Delta_u$ state with excellent Franck−Condon overlap with the $3\,^1\Pi_u$ state was the major predissociating perturber responsible for the fast second ($\tau \approx 5$ ps) channel from the results of time-resolved pump−probe spectroscopy. They reported that the observed pump−probe fluorescence signal reflected the evolution of the wavepacket in the $4\,^3\Sigma_u^+$ state and the $3\,^1\Sigma_u^+$ shelf state as well as the $3\,^1\Pi_u$ and $1\,^3\Delta_u$ states.[5] Also, long-range interaction among the $1\,^3\Delta_u$, $2\,^1\Pi_u$, and $2\,^3\Pi_u$ states was proposed by Zhang et al.[4] in order to rationalize both their assignment of the predissociating perturber and the atomic fluorescence yields measured by Breford and Engelke.[3] In the Rb₂ 430 nm system, there are three bound states, $3\,^1\Sigma_u^+$, $3\,^3\Pi_u$, and $3\,^1\Pi_u$ in the Franck−Condon region from the X $^1\Sigma_g^+$ v″ = 0 level, and several continuum states ($2\,^1\Pi_u$, $2\,^3\Pi_u$, $3\,^3\Sigma_u^+$, and $1\,^3\Delta_u$ states) corresponding to the $4\,^2D_{5/2,3/2} + 5\,^2S_{1/2}$ limits can contribute to the predissociation dynamics.[1,15] The bound excited states overlapping the $3\,^1\Pi_u$ state, however, have not yet been identified, and the combined interpretation of the previous works[3−5] on the predissociation suggests that there is a subtler dynamics due to long-range potential interaction.[4]

In this work, we present the assignments of four excited electronic states of Rb₂, $3\,^1\Pi_u$, $3\,^1\Sigma_u^+$, $3\,^3\Pi_u(0_u^+)$, and $3\,^3\Pi_u$-

---

* To whom correspondence should be addressed. E-mail: bongsoo@kaist.ac.kr. Fax: +82-42-869-2810.
[†] Advanced Photonics Research Institute.
[‡] Kyunghee University.
[§] KAIST.

(1_u), and their predissociation dynamics near 430 nm. We have obtained mass-resolved resonance enhanced two-photon ionization (RE2PI) spectra of three isotopomers of Rb₂ (^{85}Rb₂, ^{85}Rb^{87}Rb, and ^{87}Rb₂) and ^{85}Rb photofragment yield (PFY) spectrum in a very cold molecular beam (T_{vib} < 5 K and $T_{rot} \approx$ 2 K). Our greatly simplified mass-resolved spectra enabled us to identify the four excited electronic states making up the complicated vibronic structure through straightforward analysis. In our ^{85}Rb PFY spectrum, the sharp energy threshold of the fast predissociation channel is located between the isotopically shifted 3 $^1\Pi_u$ v′ = 14 levels of ^{85}Rb₂ and ^{85}Rb^{87}Rb. This reveals that the predissociating perturber corresponds to the 4 ^{2}D$_{5/2}$ + 5 ^{2}S$_{1/2}$ atomic fine-structure limit. Between the possible candidate continuum states, 1 $^3\Delta_u$ and 3 $^3\Sigma_u^+$, corresponding to the 4 ^{2}D$_{5/2}$ + 5 ^{2}S$_{1/2}$ limit, we assign the 1 $^3\Delta_u$ state to the predissociating perturber from the calculations of the relative bound (3 $^1\Pi_u$) → continuum (1 $^3\Delta_u$ or 3 $^3\Sigma_u^+$) predissociation rates. Also, we have observed the slight deviation of ^{85}Rb PFY from the prediction of Franck−Condon principle in predissociation just above the fast predissociation energy threshold. This provides the strong experimental evidence confirming the previously proposed long-range dissociation channel mixing.[4] Consequently, the fast predissociation channel branches out into two finer product channels above the higher-lying 4 ^{2}D$_{3/2}$ + 5 ^{2}S$_{1/2}$ limit.

2. Experimental Section

Our experimental apparatus and techniques have been discussed previously.[2] Briefly, we prepared Rb₂ by expanding Rb vapor with Ar gas (stagnation pressure, 760 Torr) through a modified fuel injection valve. The temperature of the nozzle was maintained at 330 °C in this experiment. The nozzle diameter was 800 μm. The pulsed jet was collimated by a 1.2 mm diameter skimmer located 7 cm from the nozzle. Rb₂$^+$ ions were generated by the absorption of two photons from a dye laser (Lambda Physik Scanmate 2E) pumped by the third harmonic of a Nd:YAG laser (Spectra Physics GCR-150). Photofragmented Rb atoms were ionized simultaneously with the excited Rb₂ by the dye laser. The ions were detected by a time-of-flight (TOF) mass spectrometer. Since Rb has two naturally occurring isotopes, Rb₂ has three different isotopomers (^{85}Rb₂, 52.1%; ^{85}Rb^{87}Rb, 40.2%; ^{87}Rb₂, 7.8%), which are well separated by our TOF mass spectrometer ($m/\Delta m \sim 500$). The line width of the dye laser is 0.12 cm^{-1}. The wavelength of the dye laser was calibrated by the Burleigh WA-4500 wavemeter and Ne optogalvanic spectrum.

3. Results and Discussion

3.1. **Assignments of the Excited States.** Figure 1 shows the ab initio potential curves of Rb₂ for ungerade states of which T_e's are located between 5s + 5p and 5s + 6s atomic limits.[1] The zero of the axis of ordinate, "Energy", in Figure 1 is set to the potential minimum of the X $^1\Sigma_g^+$ state. There are three bound potential curves of the 3 $^1\Pi_u$, 3 $^1\Sigma_u^+$, and 3 $^3\Pi_u$ states which can be excited through the vertical transition from the X $^1\Sigma_g^+$ v″ = 0 level near 430 nm (see the vertical dotted line in Figure 1). We obtained mass-resolved RE2PI spectra of three isotopomers (^{85}Rb₂, ^{85}Rb^{87}Rb, and ^{87}Rb₂) of Rb₂ between 22488 and 23788 cm^{-1}. Figure 2 shows the RE2PI spectrum of ^{85}Rb₂. We could identify five vibrational progressions, A, B, B′, C, and D as indicated in Figure 2. The abscissa label, "Frequency", in Figure 2 and the following figures represents the excitation laser frequency. Therefore, the zero-point vibrational energy $G_{v″=0}$ in the X $^1\Sigma_g^+$ state added to the frequency at which a vibronic
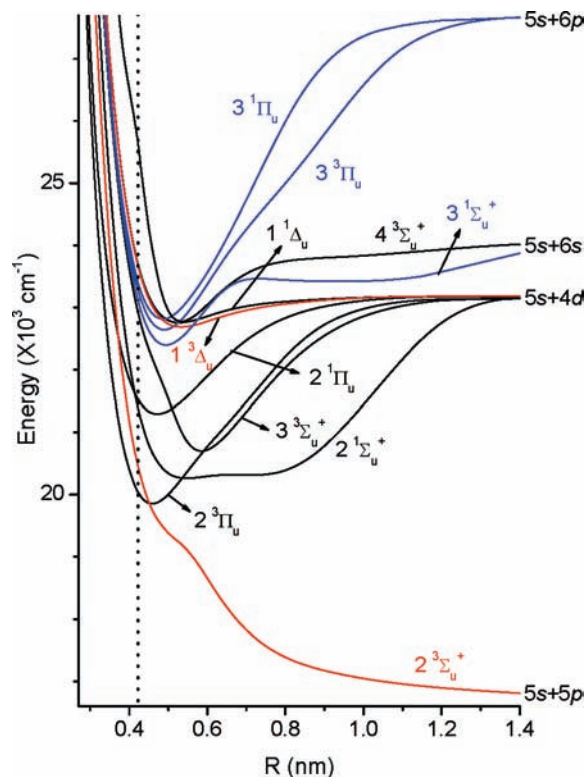

Figure 1. Ab initio potential curves of Rb₂ for ungerade states of which T_e's are located between 5p + 5s and 5s + 6s atomic limits from ref 1. The abscissa label, R, represents the internuclear distance. The ordinate energy scale is from the potential minimum of the X$^1\Sigma_g^+$ state.

band is observed in our RE2PI spectrum makes the vibrational term value, $T_{v'}$ of the excited state. This $T_{v'}$ value can be compared directly with the "Energy" of the ab initio potential curves shown in Figure 1. Mass-resolved RE2PI spectra and the observed $T_{v'}$ values of ^{85}Rb₂, ^{85}Rb^{87}Rb, and ^{87}Rb₂ can be found in the Supporting Information. The vibrational quantum numbers of A, B, C, and D progressions were assigned, as indicated in Figure 2. The observed band positions were analyzed by fitting the data sets of three Rb₂ isotopomers simultaneously using the following simple mass-reduced relation:

$$T_v = T_e + \omega_e \rho(v + {}^1\!/_2) - \omega_e x_e [\rho(v + {}^1\!/_2)]^2$$

The constant ρ (=1 for ^{85}Rb₂, 0.994237765 for ^{85}Rb^{87}Rb, and 0.988441938 for ^{87}Rb₂)[16] is given by $\rho = \sqrt{\mu/\mu_i}$, where μ is the reduced mass of the major isotopomer, ^{85}Rb₂, and μ_i represents those of ^{85}Rb^{87}Rb and ^{87}Rb₂. We truncated the higher anharmonic vibrational constants, $\omega_e y_e$, $\omega_e z_e$, etc., because the determination of the molecular constants, T_e, ω_e, and $\omega_e x_e$, is sufficient for the assignment of the electronically excited states in comparison with the results of ab initio calculation. With this limitation, the vibronic bands in the ranges of v′ = 1−25, 3−12, 4−16, and 4−18 were fitted for A, B, C, and D progressions, respectively. The vibrational quantum numbers were assigned by the isotope shifts, $\Delta T_{v'}$'s, of the vibrational bands. Since we obtained mass-resolved RE2PI spectra of ^{85}Rb₂, ^{85}Rb^{87}Rb, and ^{87}Rb₂, the absolute vibrational quantum numbers could be easily found. The observed $\Delta T_{v'}$'s should agree with the calculated values from the vibrational constants, ω_e and $\omega_e x_e$ experimentally determined when the vibrational numbering is correct. Figure 3 compares the observed $\Delta T_{v'}$'s ($T_{v'}$ of ^{85}Rb₂ − $T_{v'}$ of ^{85}Rb^{87}Rb and $T_{v'}$ of ^{85}Rb₂ − $T_{v'}$ of ^{87}Rb₂) of A, B, C, and D progressions with the calculated values from
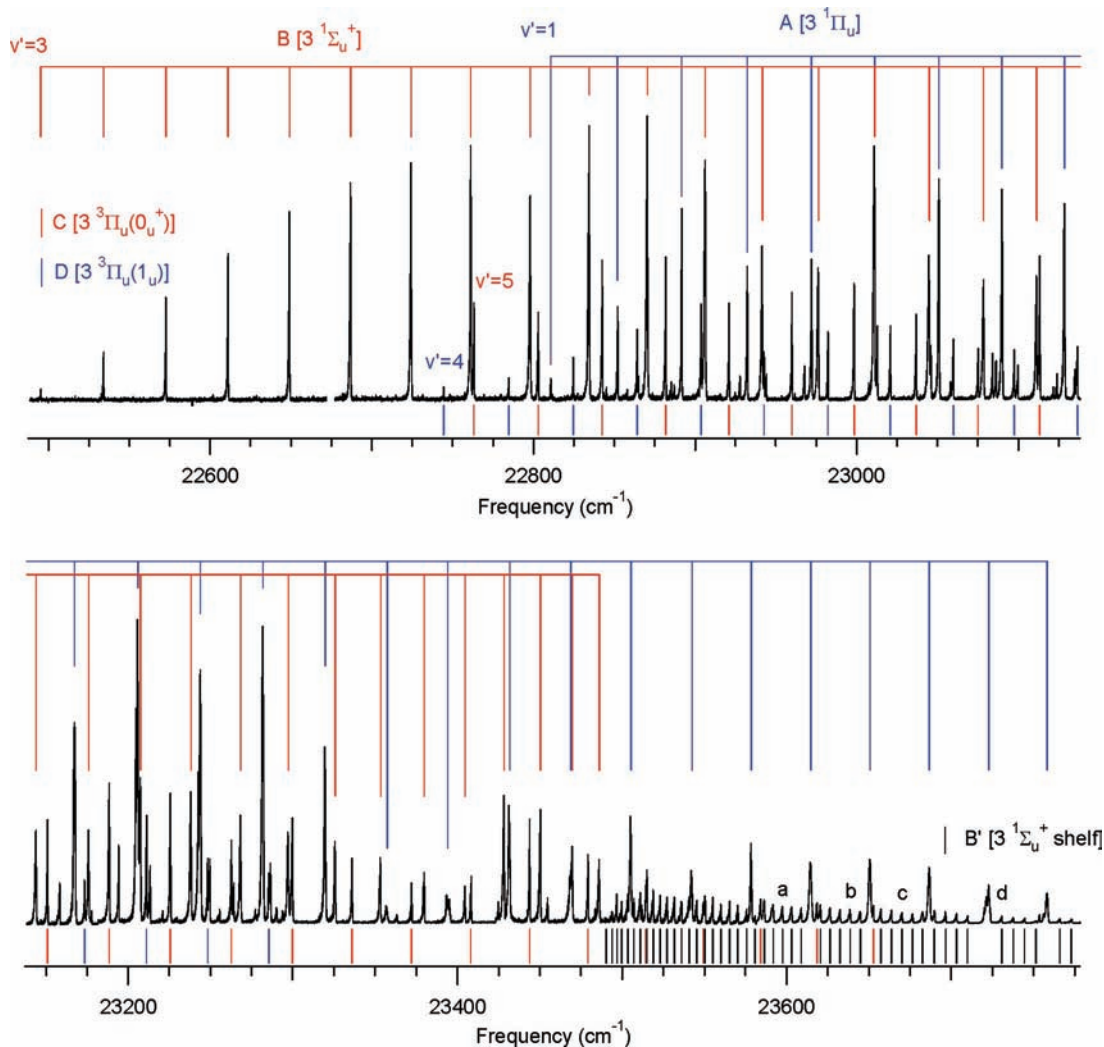
Figure 2. RE2PI spectrum of $^{85}Rb_2$. A and B progressions are indicated by red and blue sticks above the spectrum, respectively. B′, C, and D progressions are indicated by black, red, and blue sticks below the spectrum, respectively. The B′ bands of which rotational contours have been analyzed are indicated as a, b, c, and d (see text).

ω_e's and $\omega_e x_e$'s of the corresponding progressions fitted with the assignments of v''s shown in Figure 2. For the uncertainty estimate of our assignments of v''s, $\Delta T_{v'}$'s of A, B, C, and D progressions were calculated for three different vibrational numbering and compared with the observed values. The figures comparing the observed $\Delta T_{v'}$'s with the calculated values for three different vibrational numbering of A, B, C, and D progressions can be found in the Supporting Information. Over- and underestimations of v''s by $\Delta v' = \pm 1$ give the constantly larger and smaller calculated $\Delta T_{v'}$'s than the observed values in amounts of about ± 0.2 cm^{-1} between $^{85}Rb_2$ and $^{85}Rb^{87}Rb$, and ± 0.4 cm^{-1} between $^{85}Rb_2$ and $^{87}Rb_2$, respectively. These constant deviations of $\Delta T_{v'}$'s mainly come from the incorrectly determined ω_e values with the misestimated v''s used for calculating $\Delta T_{v'}$'s. However, the correct numbering gives the correct ω_e, and the deviations of the calculated $\Delta T_{v''}$'s from the observed values are less than about 0.01 cm^{-1}. The main source of the uncertainty of our assignments may arise from the fluctuation of the observed $\Delta T_{v'}$'s. This fluctuation of isotope shifts can be strong when homogeneous perturbations are extensive. In this case, the isotope shifts can enhance the irregularity of the vibrational spacing for a particular isotopomer. The fluctuation is mostly less than 0.01 cm^{-1} which is small enough for us to assign v''s correctly, and for the vibrational bands located out of the fitting region or strongly perturbed,
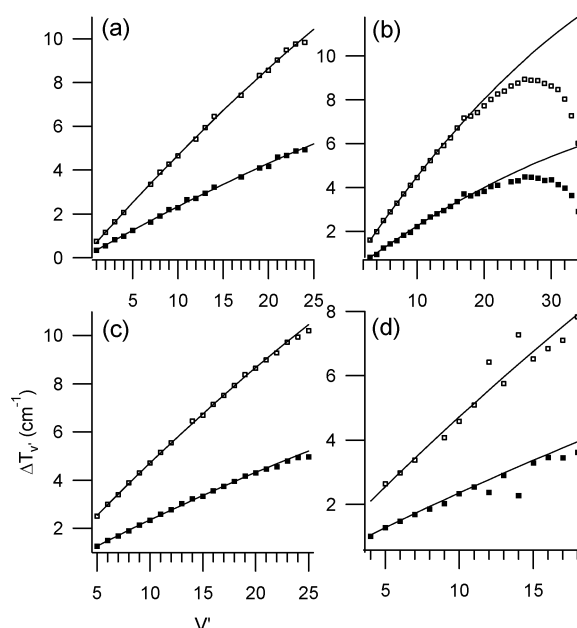
Figure 3. Isotope shifts between $^{85}Rb_2$ and $^{87}Rb_2$ (□), and between $^{85}Rb_2$ and $^{85}Rb^{87}Rb$ (■) for (a) A, (b) B, (c) C, and (d) D progressions. The solid lines indicate the expected values with the assignments of the vibrational quantum numbers shown in Figure 2.

TABLE 1: Electronic Term Values (T_e) and Vibrational Constants (ω_e and $\omega_e x_e$) of the Nine Experimentally Observed Excited States Including Our Work and Their Comparison with Theoretical Values

	expt			theory[a]		
	T_e (cm^{-1})	ω_e (cm^{-1})	$\omega_e x_e$ (cm^{-1})	T_e (cm^{-1})	ω_e (cm^{-1})	T_e(theory) $-$ T_e(expt)
A	22779.47(13)[b]	40.825(23)[b]	0.10687(82)[b]			
B	22385.139(66)[b]	40.210(18)[b]	0.1550(11)[b]			
C	22569.416(60)[b]	41.120(12)[b]	0.11154(55)[b]			
D	22589.57(22)[b]	41.400(41)[b]	0.1193(18)[b]			
3 $^1\Pi_u$	22777.5[c]	40.42[c]	0.0745[c]	22819	40	42
3 $^3\Pi_u$				22648	40	
3 $^1\Sigma_u{}^+$				22403	39	
2 $^1\Pi_u$	20895.00(2)[d]	36.406(17)[d]	0.1068(34)[d]	21301	34	406
2 $^3\Pi_u$	19784.254(9)[e]	42.000(6)[e]	0.171(1)[e]	19862	42	78
1 $^1\Delta_g$	18263.960(1)[f]	49.6652(9)[f]		18579	50	315
1 $^1\Pi_g$	15510.347(2)[d]	22.3(4)[d]	0.1486(7)[d]	15448	21	-62
1 $^1\Pi_u$	14665.64(24)[d]	47.47(13)[d]	0.143(30)[d]	14789	47	123
2 $^1\Sigma_g{}^+$	13601.57[d]	31.488(1)[d]	$-0.114(2)$[d]	13600	32	-2

a Reference 1. *b* Our work. *c* Reference 11. *d* Reference 10. *e* Reference 2. *f* Reference 14.

their v″'s could be also successfully assigned by extrapolation from the correctly assigned region. The experimentally determined molecular constants (T_e, ω_e, and $\omega_e x_e$) of A, B, C, and D progressions and those of the previously observed seven excited states are compared with the results of ab initio calculation[1] in Table 1.

The progression A has been observed between 22810 and 23760 cm^{-1}. We have assigned v′ = 1−26 ← v″ = 0 bands for ^{85}Rb₂. The assignment of the excited electronic state of A progression to the $3^1\Pi_u$ state is straightforward. T_e and ω_e of the A progression are very close to those of the $3^1\Pi_u$ state previously observed by Tsi-Zé and San-Tsiang[11] (see Table 1). As shown in Figure 2, the intensities of the vibrational bands of v′ = 15 and 16 are reduced significantly since they are strongly predissociated through the fast channel.

The candidates for the excited states of B, C, and D progressions are the $3^1\Sigma_u{}^+$ state and the $0_u{}^+$ and 1_u substates of the $3^3\Pi_u$ state. Among the three progressions, the vibrational spacings of C and D are particularly very close; the difference between T_e's of C and D progressions is 20.15 cm^{-1} and their ω_e's and $\omega_e x_e$'s are very close (see Table 1). This means that the potential energy curves of the two excited states are very similar in shape and very close to each other. Therefore, it is very probable that the upper electronic states of C and D progressions are the $3^3\Pi_u(0_u{}^+)$ and $3^3\Pi_u(1_u)$ states, respectively, which are split by spin−orbit coupling. In order to confirm these assignments, we estimated the spin−orbit coupling constant A of the $3^3\Pi_u$ state employing the atomic spin−orbit coupling parameter. Using the one-electron operator for H^{SO} and atomic spin−orbit parameters of the Rb 6p ^{2}P term, the magnitude of the spin−orbit coupling constant of the Rb₂ $3^3\Pi_u$ state can be estimated in a single-configuration approximation for the molecular electronic wavefunction.[6] The diagonal matrix element of the spin−orbit coupling operator observed as the splitting of fine-structure levels is expressed as

$$\langle\Lambda, \Sigma, S, \Omega, v|H^{SO}|\Lambda, \Sigma, S, \Omega, v\rangle = A_{\Lambda,v}\Lambda\Sigma$$

For the $^3\Pi$ state, this means that the vibrational levels of the different Ω (=0, 1, and 2) substates are equally spaced by spin−orbit coupling constant, A_v. Following the λnl notation[6] for the molecular orbital, the single-configuration representation of the electronic wavefunction of the $3^3\Pi_u$ state is $(\sigma_g 5s)(\pi_u 6p)$ omitting closed shells. The molecular spin−orbit interaction arises mainly from the electron occupying the $\pi_u 6p$ orbital. Table 2 shows the electronic quantum numbers of Λ, Σ, and Ω and

molecular orbital configurations of $^3\Pi_0$, $^3\Pi_1$, and $^3\Pi_2$. Considering only two valence electrons, H^{SO} is expressed as

$$H^{SO} = a_1\left[l_{1z}{\cdot}s_{1z} + \frac{1}{2}(l_1^+ s_1^- + l_1^- s_1^+)\right] + \\ a_2\left[l_{2z}{\cdot}s_{2z} + \frac{1}{2}(l_2^+ s_2^- + l_2^- s_2^+)\right]$$

Therefore, the diagonal matrix elements of the $^3\Pi_0$, $^3\Pi_1$, and $^3\Pi_2$ are expressed as

$$\langle^3\Pi_0|H^{SO}|^3\Pi_0\rangle = -\frac{1}{2}\langle\pi_u 6p|\hat{a}|\pi_u 6p\rangle = -\frac{1}{2}a_\pi = -A$$

$$\langle^3\Pi_1|H^{SO}|^3\Pi_1\rangle = 0$$

and
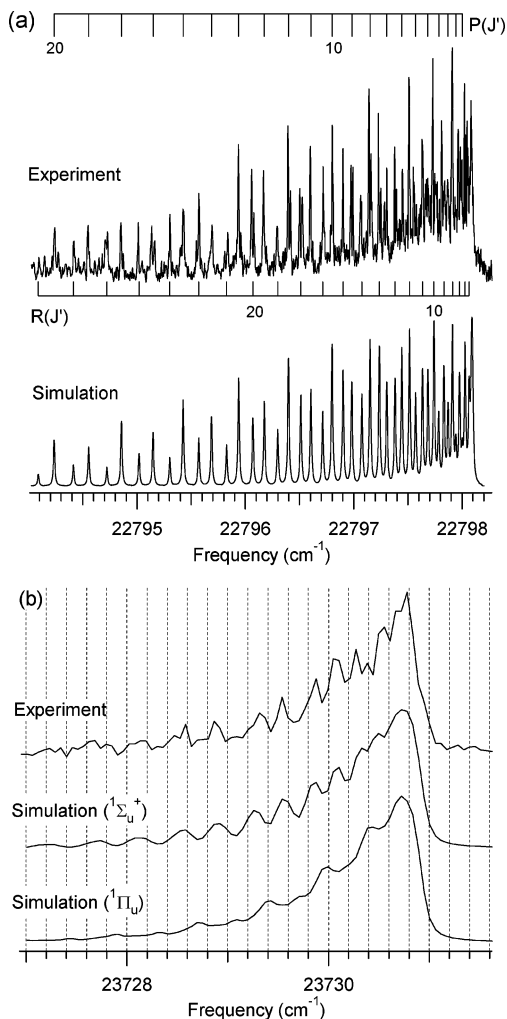
$$\langle^3\Pi_2|H^{SO}|^3\Pi_2\rangle = \frac{1}{2}\langle\pi_u 6p|\hat{a}|\pi_u 6p\rangle = \frac{1}{2}a_\pi = A$$

respectively. The atomic spin−orbit parameter ζ_{6p} is calculated as 51.67 cm^{-1} from the atomic hyperfine splitting $\Delta E = (1/2)\zeta_{6p}[J_1(J_1 + 1) - J_2(J_2 + 1)]$ and the experimentally observed value of $E_1(6p\ ^2P_{3/2}) - E_2(6p\ ^2P_{1/2}) = 77.50$ cm^{-1}.[17] The Rb₂ $3^3\Pi_u$ state correlates with the 5s + 6p limit. Therefore, the molecular $\pi_u 6p$ orbital can be expressed as linear combination of two 6p atomic orbitals. If the overlap integral of two 6p atomic orbitals is neglected, the molecular spin−orbit parameter a_π becomes equal to the atomic spin−orbit parameter ζ_{6p}. Finally, the spin−orbit coupling constant $A = (1/2)a_\pi = (1/2)\zeta_{6p} = 25.84$ cm^{-1} of the $3^3\Pi_u$ state is obtained. This estimation predicts that three spin substate of the $3^3\Pi_u$ state are equally spaced by 25.84 cm^{-1}, and the lowest substate is $^3\Pi_0$ and the highest is $^3\Pi_2$. The estimated value agrees well with the observed difference of the electronic term values between C and D progressions, 20.15 cm^{-1}. This is consistent with our assignments of the upper electronic states.

After ruling out the $3^1\Pi_u$, $3^3\Pi_u(0_u{}^+)$, and $3^3\Pi_u(1_u)$ states, the assignment of the excited state of the B progression leads to the $3^1\Sigma_u{}^+$ state. This assignment is confirmed by the

TABLE 2: Electronic Quantum Numbers and Molecular Orbital Configurations of the Substates of the 3 $^3\Pi_u$ State

| substate	Λ	Σ	Ω	molecular orbital configuration
$^3\Pi_0$	1	-1	0	$\sigma_g 5s(1)\pi_u 6p(2)\beta(1)\beta(2)$
$^3\Pi_1$	1	0	1	$\sigma_g 5s(1)\pi_u 6p(2)(1/\sqrt{2})[\alpha(1)\beta(2) + \beta(1)\alpha(2)]$
$^3\Pi_2$	1	$+1$	2	$\sigma_g 5s(1)\pi_u 6p(2)\alpha(1)\alpha(2)$

Figure 4. (a) Rotationally resolved spectrum of $^{85}Rb_2$ B v′ = 11 ←
v″ = 0 band obtained by the étalon-narrowed dye laser (upper trace)
and simulation with the fitted parameters in Table 3 (lower trace). The
molecular beam was expanded with 260 Torr of Ar. In the simulation,
we set the line width to 0.015 cm^{-1} (Lorentzian) and T_{rot} = 6 K. (b)
Partially resolved rotational contour of B′d band (top) and simulations
assuming the electronic symmetry of the upper electronic state as $^1\Sigma_u^+$
(middle) and $^1\Pi_u$ (bottom). The molecular beam was expanded with
760 Torr of Ar. The band parameters in Table 4 obtained by contour
fit were employed for the simulations.

TABLE 3: $T_{v′=11}$ and $B_{v′=11}$ of the 3 $^1\Sigma_u^+$ State of $^{85}Rb_2$ and
$^{85}Rb^{87}Rb$

	$T_{v′=11}$	$B_{v′=11}$
$^{85}Rb_2$	22826.9047(14)	0.0155364(41)
$^{85}Rb^{87}Rb$	22824.6451(17)	0.0153600(86)

^{a} All units are in cm^{-1}.

rotational analysis of the B v′ = 11 ← X $^1\Sigma_g^+$ v″ = 0 band.
Figure 4a shows the rotationally resolved spectrum of the B v′
= 11 ← X $^1\Sigma_g^+$ v″ = 0 band of $^{85}Rb_2$ and the simulation. Table
3 shows the $T_{v′=11}$ and $B_{v′=11}$ of $^{85}Rb_2$ and $^{85}Rb^{87}Rb$, which
were determined by a least-squares fit of 30 observed lines for
$^{85}Rb_2$ and 17 lines for $^{85}Rb^{87}Rb$ using the PGOPHER program.[18]
The rotational constants ($B_{v″=0}$ and $D_{v″=0}$) of the lower X $^1\Sigma_u^+$
v″ = 0 level were fixed as reported by Seto et al.[7] The observed
rotational structure consists of *P*- and *R*-branch rotational lines,
which is typical for the parallel transition ($\Delta\Omega$ = 0). It is
consistent with our assignment of the upper electronic state of
the B progression as the 3 $^1\Sigma_u^+$ state.
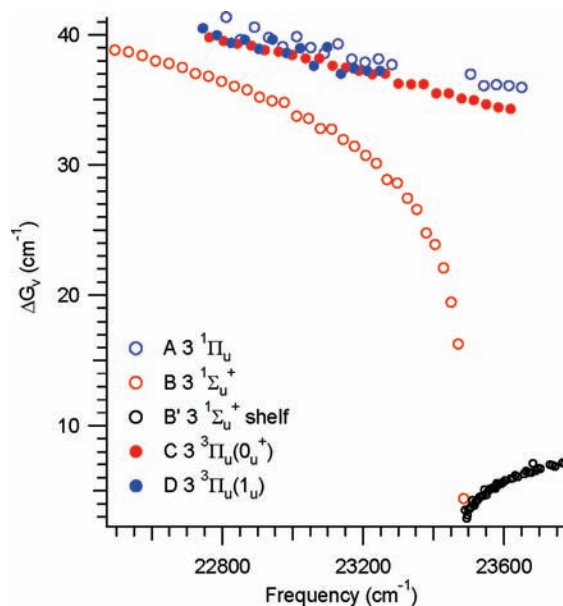
Figure 5. Plot of $\Delta G_{v′}$ of $^{85}Rb_2$ versus frequency for A, B, B′, C, and
D progressions.

**TABLE 4: Optimized Band Parameters of B′ Bands by
Rotational Contour Fit**

	B′a	B′b	B′c	B′d
band origin (cm^{-1})	23597.52(4)	23638.79^a	23670.32^a	23730.88(6)
B' (cm^{-1})	0.0058(2)	0.0059(2)	0.0057(1)	0.0060(1)
$\langle R \rangle^b$ (Å)	8.3	8.2	8.3	8.2
$\Gamma_{Gauss}{}^c$ (cm^{-1})	0.12	0.12	0.12	0.12
$\Gamma_{Lorentz}$ (cm^{-1})	0.21(2)	0.19(1)	0.14(1)	0.08(1)
τ^d (ps)	25	28	38	65
T_{rot} (K)	1.49(4)	1.60(4)	1.69(4)	1.65(6)

*^{a} Fixed. ^{b} Equilibrium bond length at the vibrational level calculated
from $\langle R \rangle = \sqrt{(\hbar^2/2)(1/hc)(1/\mu B)}$. ^{c} Fixed to the dye laser line width.
^{d} Lifetime calculated from $\Gamma_{Lorentz}$.*

For the remaining progression of B′ which is observed above
23486 cm^{-1} with a small vibrational spacing, the upper
electronic state is assigned to the 3 $^1\Sigma_u^+$ shelf state. Gador et
al. found that the 3 $^1\Sigma_u^+$ shelf state makes a significant
contribution to the nonadiabatic dynamics of Rb$_2$ near 430 nm
by time-resolved study.[5] As shown in Figure 1, the ab initio
potential well of the 3 $^1\Sigma_u^+$ state becomes broad above 23464
cm^{-1}.[1] This is due to an avoided crossing between the $^1\Sigma_u^+$
and ionic potential curves. In this case, both vibrational spacing
and rotational constants typically become greatly reduced. The
vibrational spacing of the B′ progression gradually increases
from 3 to 7 cm^{-1} in the observed spectral region (see Figure
5). Fortunately, the small rotational constant (large $\Delta B = B″
- B′$) causes the vibrational band to become significantly red
shaded and thus enables us to observe the partially resolved
rotational structure with our dye laser resolution of 0.12 cm^{-1}
as shown in Figure 4b. In order to estimate the rotational
constants, we fitted the rotational contours of four B′ bands
observed with a relatively good signal-to-noise ratio. The B′
bands of $^{85}Rb_2$ we analyzed are indicated as a, b, c, and d in
Figure 2. The optimized band parameters are shown in Table
4. Figure 4b compares the experimental contour of the B′d band
(top) with simulations assuming the electronic symmetry of the
upper electronic state as $^1\Sigma_u^+$ (middle) and$^1\Pi_u$ (bottom). The
simulation with the $^1\Sigma_u^+$ symmetry fit the experimental contour
better, and the rotational constants of B′a to B′d bands are
determined as ~0.0059 cm^{-1} (see Table 4), which correspond
to the large equilibrium bond length of ~8.3 Å. These rotational
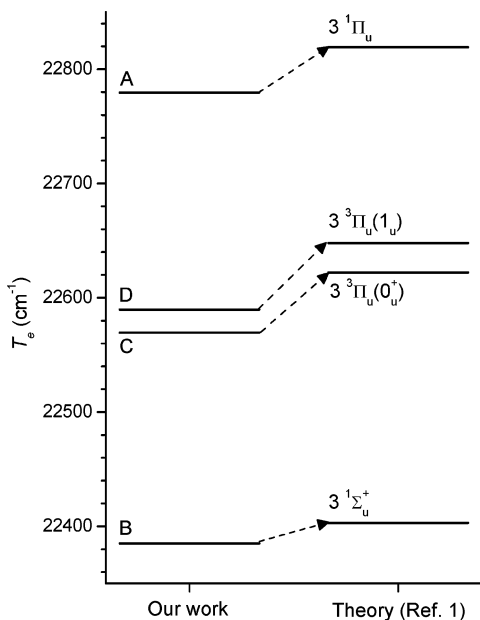
Figure 6. Comparison of the experimentally determined T_e's of A, B, C, and D progressions with the theoretically calculated T_e's of 3 $^1\Pi_u$, 3 $^1\Sigma_u^+$, 3 $^3\Pi_u$ states from ref 1. The theoretically calculated T_e of the 3 $^3\Pi_u$ state are presented for the 3 $^3\Pi_u(1_u)$ state, and for T_e of the 3 $^3\Pi_u(0_u^+)$ state, we correct the theoretically calculated T_e of the 3 $^3\Pi_u$ state by subtracting the calculated spin−orbit coupling constant, $A = 28.84$ cm^{-1} (see text).

Figure 7. TOF mass peaks of (a) Rb₂ obtained by RE2PI via the 3 $^1\Pi_u$ v′ = 9 level and (b−e) fragmented ^{85}Rb obtained simultaneously with RE2PI of ^{85}Rb₂ via the 3 $^1\Pi_u$ v′ = 9, 15, 19, and 22 levels. Δ represents the excess energy above the fast predissociation energy threshold, the 5s + 4d atomic limit.

constants of B′ bands are considerably smaller than that of the 3 $^1\Sigma_u^+$ v′ = 11 level ($B_{v'=11} = 0.0155364(41)$ cm^{-1}) (compare the values in Tables 3 and 4). Consequently, the upper electronic state of the B′ progression is assigned as the 3 $^1\Sigma_u^+$ shelf state. The lifetime of the 3 $^1\Sigma_u^+$ shelf state could be estimated from the spectral line width. In the rotational contour fits, we fixed the Gaussian component of the line width, Γ_{Gauss}, as 0.12 cm^{-1}, the resolution of our dye laser, and floated the Lorentzian component, $\Gamma_{Lorentz}$. The lifetimes were estimated to be tens of picoseconds from the fitting of $\Gamma_{Lorentz}$, and this suggests that the 3 $^1\Sigma_u^+$ state is also predissociated above the fast predissociation energy threshold like the 3 $^1\Pi_u$ state. This is consistent with our observations of the ^{85}Rb PFY from the parent Rb₂ 3 $^1\Sigma_u^+$ vibrational levels above the fast predissociation energy threshold (see section 4.2 and ^{85}Rb fragment mass spectra in the Supporting Information).

The vibrational spacings observed for the A, B, B′, C, D progressions reflect the effect of homogeneous ($\Delta\Omega = 0$) perturbation. Figure 5 shows $\Delta G_{v'}$ ($= T_{v'+1} - T_{v'}$) versus frequency for these vibrational progressions. The vibrational spacing of A and D progressions assigned to the 3 $^1\Pi_u$ and 3 $^3\Pi_u(1_u)$ state with $\Omega = 1$ symmetry, respectively, shows stronger irregularities than that of the others with $\Omega = 0$ symmetry. This suggests that there are strong homogeneous perturbations between the 3 $^1\Pi_u$ and 3 $^3\Pi_u(1_u)$ states. Breford and Engelke also indicated the irregular vibrational spacing of the 3 $^1\Pi_u$ state and proposed the mixing of the 3 $^1\Pi_u$ state with an overlapping $^3\Pi_u$ state.[3] Figure 6 summarizes our assignments of the electronic states in this spectral region. The left column shows the experimentally determined T_e's of A, B, C, and D progressions, and the right column shows the theoretically calculated T_e's of the 3 $^1\Pi_u$, 3 $^1\Sigma_u^+$, and 3 $^3\Pi_u$ states.[1] For T_e of the 3 $^3\Pi_u(1_u)$ state, the theoretically calculated T_e values of the 3 $^3\Pi_u$ state are presented, and for T_e of the 3 $^3\Pi_u(0_u^+)$ state, we correct the theoretically calculated T_e of the 3 $^3\Pi_u$ state by subtracting the calculated spin−orbit coupling constant, $A = 28.84$ cm^{-1}. The dotted arrows in Figure 6 indicate our assignments. The
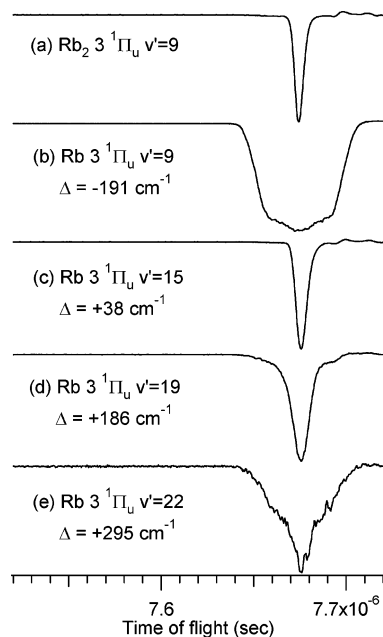
ab initio T_e's of these states are all larger than those experimentally determined by 18−58 cm^{-1}. Park et al. estimated their average deviation of T_e as about 100 cm^{-1}.[1] In Table 1, we show T_e(theory) − T_e(expt) for the previously observed seven excited states.

For the unassigned bands in our RE2PI spectrum, the candidates for their upper electronic states may be the 4 $^3\Sigma_u^+$ and 1 $^3\Delta_u$ states of which the potential curves cross those of the 3 $^1\Pi_u$ state below the 5s + 4d atomic limit. Gador et al. observed the build-up of the wavepacket in the bound potential of the 4 $^3\Sigma_u^+$ state through intersystem crossing by probing the time-resolved fluorescence signal at the outer turning point of the 4 $^3\Sigma_u^+$ state.[5] Although the bound potentials of the 4 $^3\Sigma_u^+$ and 1 $^3\Delta_u$ states are out of the Franck−Condon region (see Figure 1), some of their vibrational levels might borrow transition probability from the 3 $^1\Pi_u$ state through various couplings particularly in the region of potential crossing.

3.2. Investigation of the Predissociation Dynamics. As previously reported,[3−5] the Rb₂ 3 $^1\Pi_u$ state is predissociated into two channels. It has been known that the lower part of the 3 $^1\Pi_u$ state is predissociated into the 5 $^2S_{1/2}$ + 5 $^2P_{3/2}$ limit whereas the higher vibrational levels are strongly predissociated, $\tau \approx 5$ ps, into the 5s + 4d limit. We call the former slow and the latter fast channels, classifying by the predissociation lifetimes. Despite various kinds of studies such as the measurement of atomic fluorescence yields,[3] time-resolved pump−probe spectroscopy,[4,5] and a theoretical approach,[15] the resolution of the atomic fine-structure limit corresponding to the fast predissociation energy threshold and the assignment of the predissociating perturber for the fast channel are still in debate.

We have observed the two-channel (fast and slow) predissociation of the 3 $^1\Pi_u$ state. The two-channel predissociation can be resolved by measuring the kinetic energy of the fragmented atoms. The kinetic energy of the fragmented atoms produced by the slow channel is 6348 cm^{-1} for the 3 $^1\Pi_u$ v′ = 9 level, which is significantly larger than that produced by the fast channel. Figure 7 shows the TOF mass peaks of (a) ^{85}Rb₂

and (b–e) the fragmented ^{85}Rb. The intensities of the TOF mass peaks of ^{85}Rb (Figure 7b–e) were normalized with respect to that of ^{85}Rb$_2$ (Figure 7a). The mass peak of ^{85}Rb$_2$ was obtained by RE2PI via the 3 $^1\Pi_u$ v′ = 9 level, and those of the fragmented ^{85}Rb were obtained simultaneously with RE2PI of ^{85}Rb$_2$ via the 3 $^1\Pi_u$ v′ = 9, 15, 19, and 22 levels. Ionization of the excited Rb atoms resulting from the two predissociation channels requires photon energy at least larger than 20874.5 cm^{-1} (for the lower energy 5p Rb*), which can be achieved by the same dye laser used for RE2PI of ^{85}Rb$_2$ ($\lambda \sim$ 430 nm). The excess energy above the fast predissociation threshold (5s + 4d), Δ, is shown for each TOF mass peak. The full width at half-maximum (fwhm) and shape of ^{85}Rb TOF signal varies dramatically with the excess energy (see Figure 7b–e). The fwhm of the mass peak is determined by the initial space and kinetic energy distributions of ions. For the mass peaks shown in Figure 7, the initial space distribution of ions is the same since the laser spot size (∼2 mm) was not changed during the measurements. Typically, the fwhm of the mass peak obtained by the combination of the Wiley–McLaren type linear TOF mass spectrometer and a skimmed supersonic jet with the ionization source of a nanosecond pulsed laser is limited by laser time duration.[19] The ^{85}Rb$_2$ peak in Figure 7a shows fwhm of ∼6 ns which corresponds to the time duration of our dye laser pumped by the third harmonic of a Nd:YAG laser. When the parent dimer ^{85}Rb$_2$ is excited to the 3 $^1\Pi_u$ v′ = 9 level below the fast predissociation energy threshold, $\Delta = -191$ cm^{-1}, the fragmented ^{85}Rb shows mass peak with fwhm = 48 ns. This broad fwhm comes from the large kinetic energy released by the slow predissociation channel producing Rb 5 ^{2}P$_{3/2}$ and Rb 5 ^{2}S$_{1/2}$ fragments. The fast predissociation channel produces 5s and 4d Rb atoms with relatively small translational energy supplied by the excess energy Δ. Figure 7c shows that the fwhm of the ^{85}Rb peak in the TOF spectrum is 7 ns just above the fast predissociation threshold energy, $\Delta = +38$ cm^{-1}. From Figure 7c–e, we could find that the contribution of the ^{85}Rb mass signal with relatively larger fwhm to the TOF signal increases gradually. This suggests that the predissociation rates through the slow and fast channels become comparable as the excess energy is increased.

In our ^{85}Rb PFY spectrum, the atomic fine-structure limit corresponding to the fast predissociation energy threshold has been resolved. Figure 8a shows the ^{85}Rb PFY spectrum along with the RE2PI spectra of ^{85}Rb$_2$ and ^{85}Rb^{87}Rb. The ^{85}Rb PFY spectrum shows band structures resulting from the predissociation of both ^{85}Rb$_2$ and ^{85}Rb^{87}Rb. The ^{85}Rb$_2$ 3 $^1\Pi_u$ v′ = 14 level, the lowest level above the threshold energy (5s + 4d), is denoted with an arrow in Figure 8a. Figure 8b shows an expanded spectra around the threshold energy versus frequency + $G_{v''=0}$; 3 $^1\Pi_u$ v′ = 14 ← X $^1\Sigma_g^+$ v″ = 0 bands of ^{85}Rb$_2$ and ^{85}Rb^{87}Rb, and the corresponding ^{85}Rb PFY, are shown. The isotope shift between the 3 $^1\Pi_u$ v′ = 14 levels of ^{85}Rb$_2$ and ^{85}Rb^{87}Rb is 3.2 cm^{-1}. From the ^{85}Rb PFY spectrum, it is found that the ^{85}Rb$_2$ 3 $^1\Pi_u$ v′ = 14 level is strongly predissociated, but the isotopically down shifted ^{85}Rb^{87}Rb 3 $^1\Pi_u$ v′ = 14 level shows a very small ^{85}Rb PFY which probably results from the slow predissociation channel. Therefore, the fast predissociation threshold energy is located between these two levels. The energies of the atomic fine-structure limits of 4 ^{2}D$_{3/2}$ + 5 ^{2}S$_{1/2}$ and 4 ^{2}D$_{5/2}$ + 5 ^{2}S$_{1/2}$ are also shown together in Figure 8b. For comparison, the dissociation energy of the Rb$_2$ X $^1\Sigma_g^+$ state, 3993.53(±0.06) cm^{-1}, determined by photoassociation spectroscopy,[20] is added to the energies of the fine-structure components of Rb 4 ^{2}D$_J$. The fine structures of Rb 4 ^{2}D$_J$ are
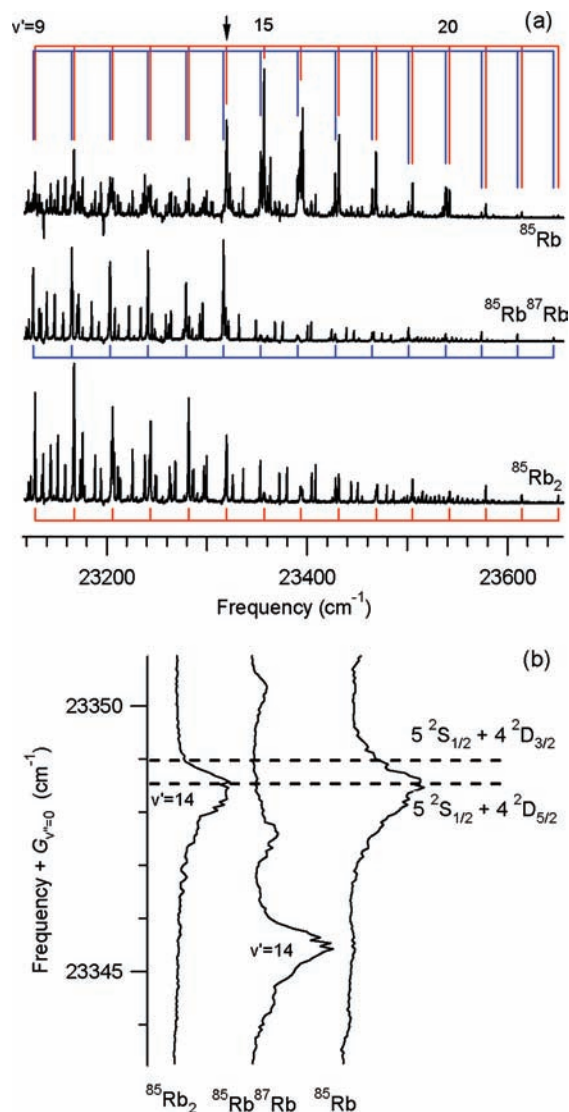
Figure 8. (a) RE2PI spectra of ^{85}Rb$_2$ and ^{85}Rb^{87}Rb and ^{85}Rb PFY spectrum between 23117.9 and 23655.5 cm^{-1} and (b) the expanded RE2PI and PFY spectra around the 5s + 4d atomic limit along with the atomic fine-structure limits of 5 ^{2}S$_{1/2}$ + 4 ^{2}D$_{3/2,5/2}$ (---). In part a, the vibrational progressions of the 3 $^1\Pi_u$ state are indicated by red and blue sticks for ^{85}Rb$_2$ and ^{85}Rb^{87}Rb, respectively, and the arrow indicates the lowest vibrational level, v′ = 14, of the 3 $^1\Pi_u$ state predissociated into the fast channel. For the direct comparison of the observed fast predissociation threshold with the atomic fine-structure limits in part b, the RE2PI and PFY spectra are shown with respect to the frequency + $G_{v''=0}$ and the dissociation energy of the X $^1\Sigma_g^+$ state are added to the atomic fine-structure energy.

inverted in energy, and thus, the energy level of 4 ^{2}D$_{3/2}$ is higher than that of 4 ^{2}D$_{5/2}$ by 0.44 cm^{-1}.[17] Between the two fine-structure limits of 5s + 4d, the lower-lying 5 ^{2}S$_{1/2}$ + 4 ^{2}D$_{5/2}$ is located just below the ^{85}Rb$_2$ 3 $^1\Pi_u$ v′ = 14 level. However, the higher-lying 5 ^{2}S$_{1/2}$ + 4 ^{2}D$_{3/2}$ is located above the ^{85}Rb$_2$ 3 $^1\Pi_u$ v′ = 14 level. Consequently, we assign the fast predissociation energy threshold to the lower-lying 5 ^{2}S$_{1/2}$ + 4 ^{2}D$_{5/2}$ limit.

There are two possible candidates, 1 $^3\Delta_u$ and 3 $^3\Sigma_u^+$, for the predissociating perturber responsible for the fast channel of the 3 $^1\Pi_u$ state. They correspond to the 5 ^{2}S$_{1/2}$ + 4 ^{2}D$_{5/2}$ fine-structure limit and can be mixed with the 3 $^1\Pi_u$ state via spin–orbit coupling ($\Delta\Omega = 0$). To assign the predissociating perturber, we calculated the relative predissociation rates of the 3 $^1\Pi_u$ state by two possible perturbers, 1 $^3\Delta_u$ and 3 $^3\Sigma_u^+$, using the BCONT 2.0 program[21] and compared them with the observed ^{85}Rb PFY spectrum. The ab initio potential energy
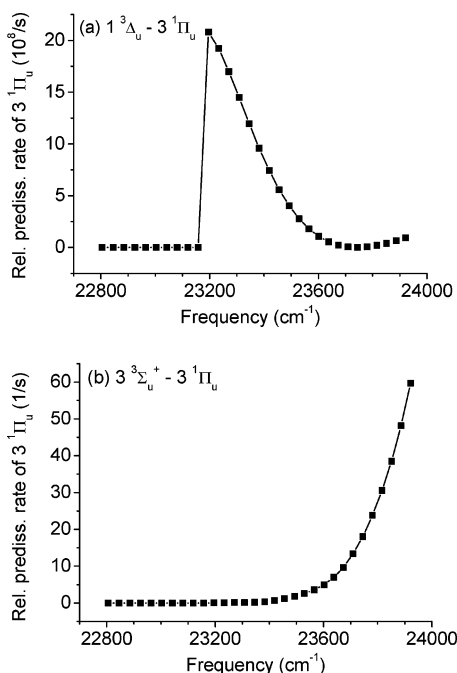
Figure 9. Relative predissociation rates of the 3 $^1\Pi_u$ state into the continuum (a) 1 $^3\Delta_u$ and (b) 3 $^3\Sigma_u^+$ states calculated assuming the bound-continuum spin−orbit coupling constants of both cases as 1 cm^{-1}. For the calculation, ab initio potential curves of the 3 $^1\Pi_u$, 1 $^3\Delta_u$, and 3 $^3\Sigma_u^+$ states were employed from ref 1.

curves of the 3 $^1\Pi_u$, 1 $^3\Delta_u$, and 3 $^3\Sigma_u^+$ states accurate within a few tens of cm^{-1} were used from the work by Park et al.[1] For the H^{SO} between the 3 $^1\Pi_u$ and 1 $^3\Delta_u$ state, Zhang et al. estimated 10 cm^{-1} from their measurement of the predissociation lifetime (5 ps),[4] and Edvardsson et al. predicted 4−5 cm^{-1} theoretically.[15] However, the accurate $H^{SO}(R)$ functions of 3 $^1\Pi_u$ − 1 $^3\Delta_u$ and 3 $^1\Pi_u$ − 3 $^3\Sigma_u^+$ are still unavailable. Therefore, we set the H^{SO} of both 1 $^3\Delta_u$ − 3 $^1\Pi_u$ and 3 $^3\Sigma_u^+$ − 3 $^1\Pi_u$ to be 1 cm^{-1}, and thus the relative predissociation rate we calculate can be interpreted as the bound-continuum radial overlap integral. Figure 9 shows the calculated relative predissociation rates of 3 $^1\Pi_u$ → 1 $^3\Delta_u$ and 3 $^1\Pi_u$ → 3 $^3\Sigma_u^+$. They show strikingly different variations with the excitation energy. In the case of 1 $^3\Delta_u$ − 3 $^1\Pi_u$, the sharp energy threshold is apparent. This agrees well with the observed ^{85}Rb PFY spectrum (see Figure 8a). However, in the case of 3 $^3\Sigma_u^+$ − 3 $^1\Pi_u$, the predissociation rate increases gradually with excitation energy. Also, the radial overlap integral between the 1 $^3\Delta_u$ and 3 $^1\Pi_u$ states is calculated to be very favorable, which is greater than that between the 3 $^3\Sigma_u^+$ and 3 $^1\Pi_u$ states by ∼10^8 times. From the comparison of the observed ^{85}Rb PFY spectrum with these calculations, we assign the predissociating perturber as the 1 $^3\Delta_u$ state.

However, there is a discrepancy in the vibrational level that shows maximum ^{85}Rb PFY in our experimental PFY spectrum and that in the calculation which is shown in Figure 9a. For the ^{85}Rb$_2$ 3 $^1\Pi_u$ state, the ^{85}Rb PFY increases suddenly at the $v' = 14$ band, goes further at $v' = 15$, and then decreases afterward in the experimental PFY spectrum. According to the Franck−Condon principle in predissociation, the probability of the radiationless transition from bound to continuum states decreases as the kinetic energy becomes higher at the point of transition.[22] The result of the 1 $^3\Delta_u$ − 3 $^1\Pi_u$ calculation reflecting this principle shows that the first vibrational level of the 3 $^1\Pi_u$ state above the dissociation limit is most strongly predissociated and the predissociation becomes increasingly weaker as the vibrational level of the 3 $^1\Pi_u$ state rises (see Figure 9a). This

discrepancy can be rationalized by the long-range potential crossing between the 1 $^3\Delta_u$ state and other continuum states (2 $^1\Pi_u$ or 2 $^3\Pi_u$) corresponding to the higher-lying 5 $^2S_{1/2}$ + 4 $^2D_{3/2}$ limit. This potential crossing is unavoidable because the lower-lying electronic states correspond to the higher-lying atomic fine-structure limit. In this situation, it is very probable that the predissociation of the vibrational levels of the 3 $^1\Pi_u$ state above the higher-lying 5 $^2S_{1/2}$ + 4 $^2D_{3/2}$ limit branches out into two finer product channels, 5 $^2S_{1/2}$ + 4 $^2D_{5/2}$ and 4 $^2D_{3/2}$. For the ^{85}Rb$_2$ 3 $^1\Pi_u$ $v' = 14$ level located between 4 $^2D_{5/2}$ + 5 $^2S_{1/2}$ and 4 $^2D_{3/2}$ + 5 $^2S_{1/2}$ limits, only the lower-lying product channel is available for predissociation, and the population transferred from the 1 $^3\Delta_u$ potential to the 2 $^1\Pi_u$ or 2 $^3\Pi_u$ potentials corresponding to the higher-lying limit is reflected back to the bound region. When the long-range interaction between the 1 $^3\Delta_u$ state and other continuum states is significantly strong, the ^{85}Rb PFY from the ^{85}Rb$_2$ 3 $^1\Pi_u$ $v' = 14$ level becomes smaller than that from the ^{85}Rb$_2$ 3 $^1\Pi_u$ $v' = 15$.

For the newly identified states, 3 $^1\Sigma_u^+$, 3 $^3\Pi_u(0_u^+)$, and 3 $^3\Pi_u(1_u)$, the corresponding ^{85}Rb PFY below and above the threshold of the fast predissociation was obtained (see Figure 8). Also, the lifetime of the 3 $^1\Sigma_u^+$ state is estimated to be significantly short above the 5s + 4d atomic limit (see section 3.1). It is probable that the four bound excited states, 3 $^1\Pi_u$, 3 $^1\Sigma_u^+$, 3 $^3\Pi_u(0_u^+)$, and 3 $^3\Pi_u(1_u)$, in this spectral region may be mixed by homogeneous and heterogeneous perturbations and the predissociation of the $\Omega = 0$ states becomes possible through $\Omega = 1$ doorway states.

4. Conclusion

We have assigned four electronically excited states, 3 $^1\Pi_u$, 3 $^1\Sigma_u^+$, 3 $^3\Pi_u(0_u^+)$, and 3 $^3\Pi_u(1_u)$, making up the complex vibronic structure of the Rb$_2$ 430 nm system. Their T_e's, ω_e's, and $\omega_e x_e$'s have been determined by vibrational analysis of the observed band progressions. For predissociation dynamics, the established slow and fast channels[3,4] have been resolved independently by the fwhm of the fragmented ^{85}Rb$^+$ mass peak. For the fast channel, the corresponding atomic fine-structure limit has been identified. This observation combined with the theoretical prediction of the relative predissociation rates of the ^{85}Rb$_2$ 3 $^1\Pi_u$ state into 1 $^3\Delta_u$ and 3 $^3\Sigma_u^+$ continua identifies the predissociating perturber responsible for the fast channel as the 1 $^3\Delta_u$ state. Our assignments of the bound and continuum states contributing to the complicated vibronic spectrum and the predissociation dynamics in the Rb$_2$ 430 nm system are consistent with the previous frequency[3]- and time[4,5]-domain spectroscopic studies. Also, we provide the experimental evidence for the long-range dissociation channel mixing previously proposed,[4] which results in branching out of the fast channel into two finer product channels. The long-range dissociation channel mixing due to an unavoidable potential crossing between the 1 $^3\Delta_u$ state and other continuum state corresponding to the different atomic fine-structure limits provides coherent rationalization of the three independent experimental results of atomic fluorescence yield measurement,[3] time-resolved pump−probe spectroscopy,[4] and our photofragment yield measurement.

Our study of the Rb$_2$ 430 nm system encourages high-resolution experiments and deperturbation analysis which will provide accurate potential curves of the excited states and the coupling constants among them. These will lead to comprehensive and deeper understanding of the electronic structure and predissociation dynamics of Rb$_2$ in this spectral region.

Supporting Information Available: Data of the Rb_2 3 $^1\Pi_u$, 3 $^1\Sigma_u^+$, 3 $^3\Pi_u(0_u^+)$, and 3 $^3\Pi_u(1_u)$ states by RE2PI and PFY spectroscopy: (i) mass-resolved RE2PI spectra and (ii) observed vibrational term values, $T_{v'}$, of $^{85}Rb_2$, $^{85}Rb^{87}Rb$, and $^{87}Rb_2$, (iii) observed isotope shifts, $\Delta T_{v'}$, compared with the calculated values, and (iv) TOF mass spectra of fragmented ^{85}Rb obtained by exciting $^{85}Rb_2$ to the 3 $^1\Sigma_u^+$ state. This material is available free of charge via the Internet at http://pubs.acs.org.

References and Notes

(1) Park, S. J.; Suh, S. W.; Lee, Y. S.; Jeung, G.-H. *J. Mol. Spectrosc.* **2001**, *207*, 129.

(2) Lee, Y.; Yoon, Y.; Baek, S. J.; Joo, D.-L.; Ryu, J.; Kim, B. *J. Chem. Phys.* **2000**, *113*, 2116.

(3) Breford, E. J.; Engelke, F. *Chem. Phys. Lett.* **1980**, *75*, 132.

(4) Zhang, B.; Berg, L.-E.; Hansson, T. *Chem. Phys. Lett.* **2000**, *325*, 577.

(5) Gador, N.; Zhang, B.; Andersson, R.; Johansson, P.; Hansson, T. *Chem. Phys. Lett.* **2003**, *368*, 202.

(6) Lefebvre-Brion, H.; Field, R. W. *The Spectra and Dynamics of Diatomic Molecules*; Elsevier: New York, 2004.

(7) Seto, J. Y.; Le Roy, R. J.; Vergès, J.; Amiot, C. *J. Chem. Phys.* **2000**, *113*, 3067.

(8) Amiot, C. *Mol. Phys.* **1986**, *58*, 667.

(9) Amiot, C.; Vergès, J. *Mol. Phys.* **1987**, *61*, 51.

(10) Amiot, C. *J. Chem. Phys.* **1990**, *93*, 8591.

(11) Tsi-Zé, N.; San-Tsiang, T. *Phys. Rev.* **1937**, *52*, 91.

(12) Brom, J. M.; Jr.; Broida, H. P. *J. Chem. Phys.* **1974**, *61*, 982.

(13) Feldman, D. L.; Zare, R. N. *Chem. Phys.* **1976**, *15*, 415.

(14) Yoon, Y.; Lee, Y.; Lee, S.; Kim, B. *J. Chem. Phys.* **2002**, *116*, 6660.

(15) Edvardsson, D.; Lunell, S.; Marian, C. M. *Mol. Phys.* **2003**, *101*, 2381.

(16) Mills, I.; Cvitaš, T.; Homann, K.; Kallay, N.; Kuchitsu, K. *Quantities, Units and Symbols in Physical Chemistry*; Blackwell: Oxford, 1993.

(17) Moore, C. E. *Atomic Energy Levels*; National Bureau of Standands (U.S.) GPO: Washington, D.C., 1971; Circ. 35; Vol. I.

(18) Western, C. M. *PGOPHER version 5.2, a Program for Simulating Rotational Structure*; University of Bristol, 2007; http://pgopher.chm-.bris.ac.uk.

(19) Lubman, D. M.; Jordan, R. M. *Rev. Sci. Instrum.* **1985**, *56*, 373.

(20) Tsai, C. C.; Freeland, R. S.; Vogels, J. M.; Boesten, H. M. J. M.; Verhaar, B. J.; Heinzen, D. J. *Phys. Rev. Lett.* **1997**, *79*, 1245.

(21) Le Roy, R. J.; Kraemer, G. T. *BCONT 2.0. A Computer Program for Calculating Bound → Continuum Transition Intensities for Diatomic Molecules*; University of Waterloo Chemical Physics Research Report CP-650R; 2001.

(22) Herzberg, G. *Molecular Spectra and Molecular Structure I. Spectra of Diatomic Molecules*, 2nd ed.; Krieger: Malabar, 1989.